

Active mechanics reveal molecular-scale force kinetics in living oocytes

May 17, 2022

Wylie W. Ahmed^{1,2,7}, Etienne Fodor^{3,7}, Maria Almonacid^{4,7}, Matthias Bussonnier², Marie-Helene Verlhac⁴, Nir Gov⁵, Paolo Visco³, Frederic van Wijland³, Timo Betz^{2,6}

1 Department of Physics, California State University, Fullerton, California 92831, USA

2 Laboratoire Physico Chimie Curie, Institut Curie, PSL Research University, CNRS UMR168, 75005, Paris, France; Sorbonne Universités, UPMC Univ Paris 06, 75005, Paris, France

3 Laboratoire Matiere et Systemes Complexes, UMR 7057, Universite Paris Diderot, 75013 Paris, France

4 CIRB, College de France, and CNRS-UMR7241 and INSERM-U1050, Equipe Labellisee Ligue Contre le Cancer, Paris F-75005, France

5 Department of Chemical Physics, Weizmann Institute of Science, 76100 Rehovot, Israel

6 Institute of Cell Biology, Center for Molecular Biology of Inflammation, Cells-in-Motion Cluster of Excellence, Münster University, Von-Esmarch-Strasse 56, D-48149 Münster, Germany

7 equally contributing authors

Abstract

Active diffusion of intracellular components is emerging as an important process in cell biology. This process is mediated by complex assemblies of molecular motors and cytoskeletal filaments that drive force generation in the cytoplasm and facilitate enhanced motion. The kinetics of molecular motors have been precisely characterized *in-vitro* by single molecule approaches, however, their *in-vivo* behavior has remained elusive. Here, we study the myosin-V driven active diffusion of vesicles in mouse oocytes, where this process plays a key role in nuclear positioning during development, and combine an experimental and theoretical framework to extract molecular-scale force kinetics *in-vivo* (motor force, power-stroke, and velocity). We find that myosin-V induces rapid kicks of duration $\tau \sim 300 \mu\text{s}$ resulting in an average force of $F \sim 0.4 \text{ pN}$ on vesicles. Our results reveal that measuring *in-vivo* active fluctuations allows extraction of the underlying molecular motor activity and demonstrates a widely applicable mesoscopic framework to access molecular-scale force kinetics.

1 Introduction

Living cells utilize motor proteins to actively generate force at the molecular scale to drive motion and organization in the crowded intracellular environment [1–4]. For example, force generation is critical to facilitate the basic tasks of living cells such as spatial organization, motility, division, and organelle transport. Recently, "active diffusion" has emerged as an important process in cell biology [5–9]. Active diffusion is the random motion of intracellular components that is driven by active metabolically powered forces (and not by thermal fluctuations). An interesting example occurs during early vertebrate development, namely oocyte meiosis [5].

Oocytes are immature female gametes that are destined to be fertilized and grow into a fully functioning organism. They are large cells ($80 \mu\text{m}$ in diameter) of spherical geometry with a thick actin-rich cortex and a well separated cytoplasmic-skeleton (Fig. 1A). The cytoplasmic-skeleton of a mouse oocyte is a composite material that includes actin filaments, microtubules, and intermediate filaments. The actin network is composed of long unbranched filaments polymerized from the surface of vesicles that harbor actin nucleating factors [10]. These vesicles act as nodes to create an inter-connected actin network that is uniform in density

throughout the cytoplasm and un-polarized [11]; Microtubules are organized in small seeds and do not form long filaments during prophase-I [12]; And while it is probable that intermediate filaments are present [13], little is known about their structure or function in mouse oocytes.

Correct nuclear positioning during prophase-I requires precise spatial and temporal coordination of the cytoskeleton and molecular motors [11, 14]. Recent work has shown the importance of mechanical processes in oocyte development [5, 11, 14]. Proper spindle positioning requires the oocyte cortex to soften and exhibit plastic deformation [14], and motion of the cytoplasmic actin network is closely regulated by myosin-V motors [11]. Motion of large objects, such as positioning of the spindle [14] or nucleus [5], must be driven by a physical force generated by nonequilibrium processes.

To investigate the nonequilibrium mechanical activity in living cells, it is necessary to independently measure the active molecular force generation and the local mechanical properties to understand how objects move within the complex intracellular environment. This approach was introduced to study active processes in hair bundles [15] and stress fluctuations in cells [16]. Subsequent studies utilized this concept to investigate cross-linked actin-myosin-II networks in reconstituted systems [17], beads embedded in living cells [18–21], and red blood cell membranes [22].

In this study, we measure the actively driven motion of endogenous vesicles in the largely unexplored cytoplasmic-skeleton of *in-vivo* mouse oocytes and demonstrate a general framework to quantify the underlying driving forces. We combine optical tweezer based active microrheology (AMR) and laser-tracking interferometry with our theoretical framework to quantify the *in-vivo* active mechanical processes and relate them to the underlying force kinetics. To study the activity in mouse oocytes, we examine the cytoplasmic-skeleton during prophase-I, when the actin-myosin-V network is the dominant source of activity. While this network is the key element that generates force for nuclear positioning [5], the underlying physical processes are not well understood. By using statistical mesoscopic measurements on endogenous vesicles, and theoretical modeling, we are able to extract the molecular-scale force kinetics (power-stroke duration and length, force, and velocity) of *in-vivo* myosin-V.

2 Materials and Methods

2.1 Oocyte Preparation

Oocytes were collected from 11 week old mice OF1, 13 week old C57BL6 (WT) or 15 week old *Fmn2*^{-/-} female mice as previously described [23] and maintained in Prophase I arrest in M2+BSA medium supplemented with 1 μ M Milrinone [24]. Live oocytes were embedded in a collagen gel to stop movement of the overall cell during measurements. Collagen gel was made by mixing M2 medium (33.5 μ L), 5X PBS (10 μ L), NaOH (1M, 0.9 μ L), collagen (3.6 mg/mL, 55.6 μ L) to obtain 100 μ L of the final collagen solution at 2 mg/mL with a pH \sim 7.4. 20 μ L of the collagen solution was deposited on a coverslip and live oocytes were added. The droplet was covered with another glass coverslip using Dow Corning vacuum grease to minimize evaporation. The collagen gel containing oocytes was polymerized in a humid environment at 37 $^{\circ}$ C for 30 minutes.

2.2 *Fmn2*^{-/-} and Myosin-V dominant negative

To study the effect of the actin-myosin-V network we utilize two conditions to independently perturb the actin cytoskeleton (*Fmn*^{-/-}) and the myosin-V activity (*MyoV*⁽⁻⁾). *Fmn*^{-/-} mouse oocytes have no detectable cytoplasmic actin filaments, as confirmed by several independent studies [14, 25–27]. The reduced cytoplasmic actin has also been confirmed via cytochalasin-D treated mouse oocytes, which exhibit the same phenotype and mechanical properties as *Fmn*^{-/-} [28] (Fig. S1). For myosin-V dominant negative experiments (*MyoV*⁽⁻⁾), oocytes were injected with cRNAs using an Eppendorf Femtoject microinjector as published previously [5]. Oocytes were kept in prophase-I arrest for 1-3 hours to allow expression of fusion proteins. The myosin-Vb dominant negative construct corresponds to a portion of the coiled-coil region of the myosin-Vb that mediates dimerization of the motor [10]. We believe this construct binds to the coiled-coil region of endogenous myosin-Vb resulting in impaired motor dimerization. Thus, myosin-Vb is still able to bind to vesicles and actin filaments but cannot actively generate force. It is specific to myosin-Vb and has been shown to stop vesicle motion in mouse oocytes as efficiently as brefeldin A (BFA), which is a general traffic inhibitor [5].

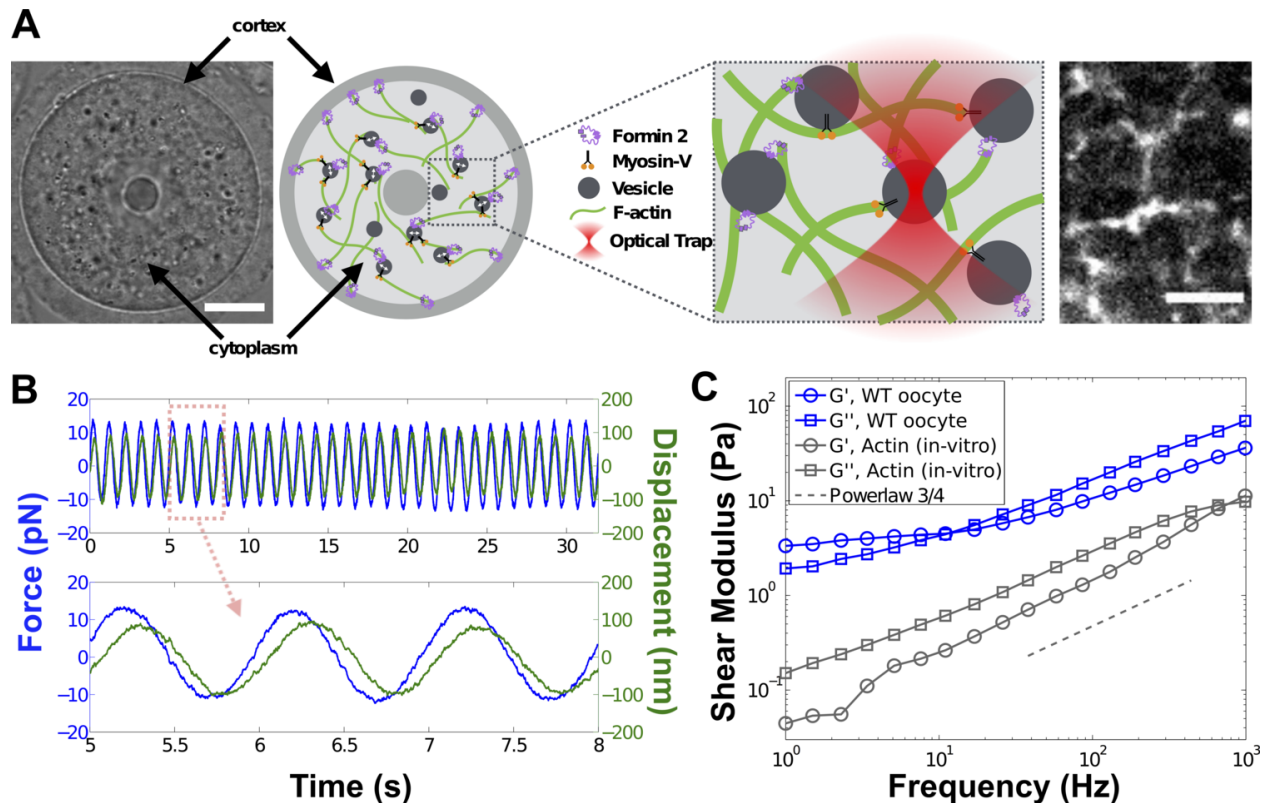


Figure 1: **Intracellular mechanics surrounding endogenous vesicles in living oocytes.** (A) Mouse oocytes are large spherical cells that have a well separated cortex and cytoplasmic-skeleton composed of biopolymer filaments (brightfield image, left)(scalebar = $20 \mu\text{m}$). During prophase-I it contains a dynamic actin-myosin-V meshwork that drives vesicle motion (schematic shown in center and fluorescent image of actin filaments on right)(scalebar = $5 \mu\text{m}$). Endogenous vesicles embedded in the cytoplasmic-skeleton are trapped using optical tweezers(zoomed inset). (B) Once a vesicle is trapped, the mechanical properties of the local environment can be measured by active microrheology (AMR) where a sinusoidal oscillating force is applied to the vesicle (blue) and the resulting displacement of the vesicle is measured (green). The viscoelastic shear modulus (G^*) is calculated from this force-displacement measurement via the Generalized Stokes-Einstein relation. (C) The mechanical properties surrounding vesicles in the cytoplasmic-skeleton of oocytes (blue) exhibits power-law behavior similar to reconstituted actin gels (gray) with frequency scaling $G^* \propto f^{0.75}$ except significantly stiffer. This shows that the cytoplasmic-skeleton in oocytes can be modeled as a semi-flexible polymer network.

2.3 *In-vitro* Actin Network Preparation

A bulk solution of actin monomers $120 \mu\text{M}$ (Cytoskeleton Inc.) was stored overnight in depolymerization buffer ($200 \mu\text{M}$ CaCl_2 , $500 \mu\text{M}$ DTT, 2mM Tris, $200 \mu\text{M}$ ATP). It was then polymerized at a final concentration of $24 \mu\text{M}$ actin in polymerization buffer (25mM Imidazol, 50mM KCl, 1mM Tris, 2mM MgCl_2 , 1mM DTT, 1mM ATP). The actin gel was polymerized between two glass coverslips at room temperature. The mesh size of the polymerized actin gel is $\sim 200 \text{nm}$ [29]. Polystyrene beads ($1 \mu\text{m}$) were embedded for optical tweezer measurements.

2.4 Optical Tweezer Setup

The optical tweezer system utilizes a near infrared fiber laser ($\lambda = 1064 \text{nm}$, YLM-1-1064-LP, IPG, Germany) that passes through a pair of acousto-optical modulators (AA-Optoelectronics, France) to control the

intensity and deflection of the trapping beam. The laser is coupled into the beam path via dichroic mirrors (ThorLabs) and focused into the object plane by a water immersion objective (60x, 1.2 NA, Olympus). The condenser is replaced by a long distance water immersion objective (40x, 0.9 NA, Olympus) to collect the light and imaged by a 1:4 telescope on a InGaAs quadrant photodiode (QPD) (G6849, Hamamatsu). The resulting signal is amplified by a custom built amplifier system (Oeffner Electronics, Germany) and digitized at a 500 kHz sampling rate and 16 bit using an analog input card (6353, National Instruments, Austin, TX, USA). All control of the experimental hardware is executed using LabVIEW (National Instruments). Optical trapping of endogenous vesicles was calibrated similarly as in [30, 31], where the high-frequency fluctuations ($f > 500$ Hz) are thermal in origin [18, 32]. For direct measurement of violation of the fluctuation dissipation theorem (FDT), laser tracking interferometry is used first to measure the spontaneous fluctuations of the vesicle, followed immediately by active microrheology to measure the mechanical properties of the local environment surrounding the vesicle.

2.5 Laser Tracking Interferometry

The position of the endogenous particle is measured by back focal plane interferometry [33]. It should be noted that deformable objects (e.g., giant unilamellar vesicles 10 – 100 μ m) undergo shape fluctuations that will manifest in the voltage measured by the QPD [34]. For small endogenous particles ($\sim 1\mu$ m), it has been confirmed that shape fluctuations are small and laser interferometry can be used to track their position with nanometer precision. This has been verified in mammalian cells [35] and yeast [36]. A recent study has also confirmed that laser tracking interferometry and the active-power spectrum calibration [30] allow quantitative force-displacement measurements on vesicles *in-vivo* [37]. To confirm the validity of this assumption in mouse oocytes we investigated the deformability of endogenous vesicles and conclude that the majority of measured fluctuations come from active vesicle displacements (see Fig. S5-10). Additionally, since the endogenous vesicles serve as nodes integrated in the cytoplasmic meshwork, they are accurate reporters of the network mechanics and fluctuations [38].

2.6 Data Analysis

In the active microrheology (AMR) experiments we apply a known force, F , to an endogenous vesicle and measure the resulting displacement, u . Using linear response theory, these are related to the material response by, $u(t) = \int_{-\infty}^t \chi(t-t')F(t')dt'$. In Fourier space we can directly calculate the complex response as $\tilde{\chi}(\omega) = \tilde{u}(\omega)/\tilde{F}(\omega)$. To translate the response function into a shear modulus we use the Generalized Stokes-Einstein relation, $G^* = 1/[6\pi R\tilde{\chi}(\omega)]$, to calculate the elastic and viscous shear moduli (G' , G'' respectively). For AMR measurements the laser power exiting the objective was ~ 120 mW. For the spontaneous fluctuations we measure the motion, $u(t)$, of endogenous vesicles via laser interferometry (without trapping the vesicle, laser power ~ 1 mW) and calculate the power spectral density (PSD), $C(\omega) = \int \langle u(t)u(0) \rangle \exp(i\omega t)dt$, as described previously [34]. Briefly, we calculate the PSD by using MATLAB (The Mathworks, USA) to take the Fast Fourier Transform (FFT) of the vesicle position, $\tilde{u} = \text{FFT}(u)$. Then the PSD is calculated as, $PSD = \frac{\tilde{u} \times \tilde{u}^*}{p \times s}$, where * denotes complex conjugate, p is the number of measurement points, and s is the sampling frequency. In systems at thermal equilibrium the response function can be calculated from the PSD via the FDT as is done for passive microrheology (PMR) [39]. Due to the particle size and linear range of the QPD measurement our PMR measurements are restricted to a particle displacement of approximately 500 nm during the measurement interval. If the particle left this regime, that part of the data was not analyzed. AMR and PMR data analysis is carried out as done previously [22].

3 Results

3.1 Intracellular mechanics of the oocyte cytoplasmic-skeleton

To measure the local mechanical properties, we optically trap an endogenous vesicle embedded in the cytoplasmic-skeleton, apply an oscillatory force while measuring its displacement (Fig 1B), and calculate the shear modulus via the Generalized Stokes-Einstein relation [40]. Since vesicles serve as integrated nodes

in the cytoplasmic-skeleton, they accurately reflect the mechanics and fluctuations of the network [38] (details on vesicle tracking in SM). To calibrate the force on the vesicles we exploit the established observation that high-frequency fluctuations are thermal in origin [18, 30, 32]. AMR directly measures the mechanical response function ($\tilde{\chi}$), which allows to determine the complex modulus (G^*) characterizing the viscous and elastic resistance of the composite cytoplasmic-skeleton including any contribution from actin, intermediate filaments, microtubules, and other structures present. We find that the cytoplasmic-skeleton of oocytes has strongly viscoelastic properties similar to semiflexible biopolymer networks (e.g. actin) [41, 42], exhibiting high-frequency power-law behavior ($G^* \propto f^\alpha$, where $\alpha \sim 0.75$) (Fig 1C). Thus, the cytoplasmic-skeleton in oocytes is strongly frequency dependent, which must be accounted for when modeling its mechanical behavior.

To dissect the mechanical contributions of cytoskeletal filaments in oocytes we first perform AMR on formin-2 knockout oocytes (Fmn -/-), which removes cytoplasmic actin filaments nucleated by formin-2 [25], as confirmed via cyto-D experiments (Fig. S1). We find that the mechanical properties do not change compared to WT, indicating that the actin network does not provide significant mechanical resistance in the oocyte (Fig. 2A, B). This behavior is presumably because the actin network in WT oocytes is sparse (Fig 1A, right and Fig. S2) with a mesh size of $5.7 \pm 1.9 \mu\text{m}$ [26]. To check this, we examine *in-vitro* reconstituted actin networks [29], which were found to be an order of magnitude softer than the oocyte (Fig 1C), thus supporting the result that WT oocyte mechanics is not dominated by the actin cytoskeleton. Depolymerizing the microtubules by nocodazole treatment ($1 \mu\text{M}$) does not significantly affect the mechanical properties (Fig. 2A, B), indicating that microtubules also do not provide significant mechanical resistance in the cytoplasmic-skeleton. This result is expected since prophase-I microtubules form small seeds instead of long force-bearing tubule structures [12]. These combined results suggest that there are other mechanical scaffolds contributing to the stiffness in the cytoplasm of mouse oocytes.

While our results show that actin does not contribute significantly to the mechanical resistance, it is known that the actin-myosin-V meshwork activity plays a critical role for self-organization such as positioning of the meiotic spindle [25, 26] and nucleus centering in mouse oocytes [5]. To independently probe the activity of this network we impaired the myosin-V motor force generation by de-activating it via microinjection of a dominant negative construct (MyoV(-))[5, 10] (see Materials and Methods). Under these conditions the mechanical properties of the cytoplasmic-skeleton stiffens significantly as evidenced by the shift upwards in the elastic and viscous moduli (Fig 2A, B). This increased mechanical stiffness correlates with a higher density actin meshwork that is observed in the absence of myosin-V activity (Fig. S2 in SM) and is readily explained by increased cross-linking [11]. This result highlights how cellular activity can be used to tune mechanical properties.

The overall behavior of the cytoplasmic-skeleton in oocytes is strongly viscoelastic where neither the elastic or viscous components dominate by a large margin. At the lowest probed frequencies the behavior is slightly more elastic with a crossover ($\sim 10 - 20 \text{ Hz}$) to more viscous at higher frequencies. However both components of the shear moduli are always within a factor of two at the observed frequencies (Fig. 2C). This is in contrast to adherent cells which typically show an overall weaker frequency dependence and are dominantly elastic[18, 43].

3.2 Quantifying *in-vivo* molecular motor activity

To quantify nonequilibrium activity we use laser-tracking to precisely measure the spontaneous motion of vesicles in the cytoplasmic-skeleton with high spatio-temporal resolution [33, 35, 36] (see Materials and Methods). Both the spontaneous motion and the local mechanics are measured for each individual vesicle. This allows direct comparison between the local environment experienced by the vesicle and the motor activity that is driving its motion. This is critical in order to extract information about the molecular-scale processes. In the absence of biochemical activity the motion of the vesicles would be due to purely thermal agitation, which is fully determined by the mechanical properties of the system. This basic relation is given by a fundamental theorem of statistical mechanics known as the fluctuation-dissipation theorem (FDT) [39]. The FDT relates the small fluctuating motion of the vesicles to the mechanical properties of the surrounding environment by, $\tilde{\chi}'' = \pi f \tilde{C} / k_B T$, where $\tilde{\chi}''$ is the dissipative part of the mechanical response, \tilde{C} is the power spectral density of vesicle motion, f is frequency, and $k_B T$ is thermal energy. However, in living cells the presence of biochemical activity gives rise to active forces (e.g. a nonequilibrium process) driven by energy

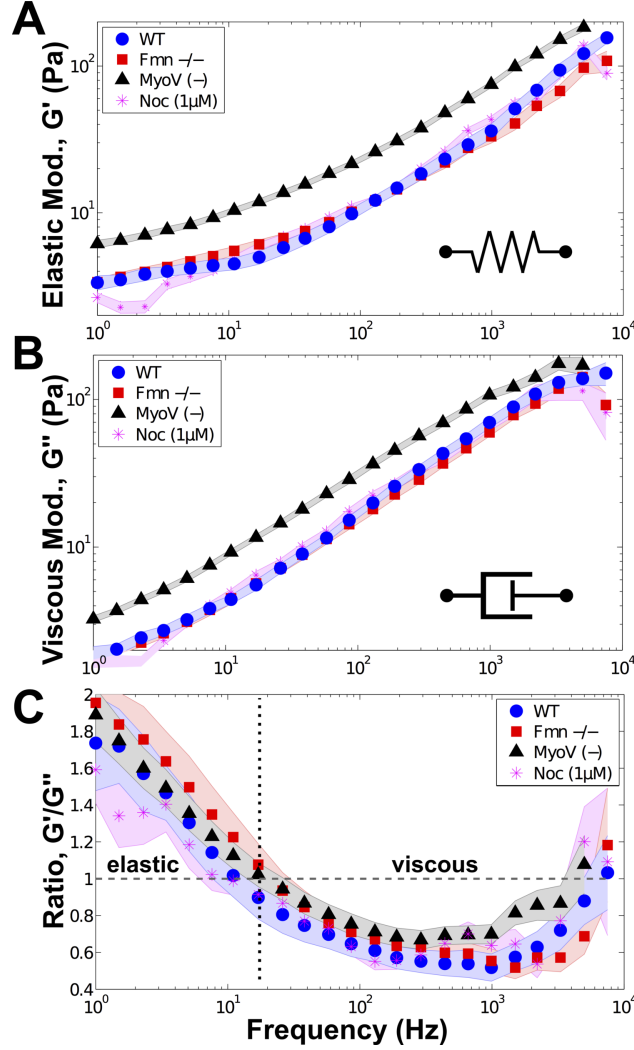


Figure 2: **The cytoplasmic-skeleton of mouse oocytes is viscoelastic.** (A, B) Insets indicate that G' quantifies the elasticity and G'' quantifies the viscous dissipation of the cytoplasmic-skeleton. The local mechanical properties (elastic and viscous) surrounding vesicles does not change from WT (blue, \circ) when actin (red \square) or microtubules (magenta $*$) are absent. However, when myosin-V is inactivated (gray \triangle), the cytoplasmic-skeleton stiffens significantly (Kolmogorov-Smirnov test, $p < 1 \times 10^{-7}$), showing that the activity driven dynamics of the actin-myosin-V meshwork maintains the soft mechanical environment surrounding vesicles in oocytes. (C) The ratio of the elastic and viscous moduli (G'/G'') in all oocytes shows that the cytoplasmic-skeleton is more elastic at lower frequencies and more viscous at higher frequencies with a crossover around $\sim 10 - 20$ Hz. This shows the highly viscoelastic nature of the oocyte cytoplasmic-skeleton. (sample size = WT: 11 cells, 32 vesicles; Fmn2: 10 cells, 33 vesicles; MyoV(-): 23 cells, 69 vesicles; Noc(1 μ M): 8 cells, 52 vesicles; shaded region indicates SEM) (note: data at 10 Hz in panel A and B are presented in a different context in [5])

consuming processes [15, 16, 44]. In other words, the force driving the motion of particles in a living cell (e.g. the oocyte) has two contributions: (1) a passive (purely thermal) contribution described by classical equilibrium physics; (2) an active contribution that is biochemically regulated and cannot be understood via equilibrium physics.

We quantify and explain both the passive and active contributions driving intracellular fluctuations, by independently measuring the response function and power spectral density. We use AMR to measure $\tilde{\chi}$

and laser-tracking to measure \tilde{C} , and use this information to check for violation of FDT [15, 17, 45], which indicates active force generation. In oocytes, at high-frequencies the mechanical response ($\tilde{\chi}''$) and the spontaneous vesicle motion ($\pi f \tilde{C}/k_B T$) are related by the FDT as expected for thermal fluctuations [18, 32] (Fig. 3A). At frequencies below ~ 400 Hz, the observed motion of vesicles is dominated by an active energy consuming process (highlighted by the pink shaded region between the two curves in Fig 3A).

To quantify the nonequilibrium activity in an active soft material it is instructive to consider the effective energy [15, 46–48], $E_{\text{eff}} = \pi f \tilde{C}/\tilde{\chi}''$, which is a measure of how far the system is from thermal equilibrium. WT oocytes exhibit a strong departure from equilibrium due mainly to the actin-myosin-V network activity. Accordingly, the deviation is reduced when either actin is absent (Fmn -/-) or myosin-V is inactivated (MyoV (-)) (Fig 3B). This is quantitative confirmation that the dynamic actin-myosin-V meshwork drives vesicle dynamics out-of-equilibrium in the cytoplasmic-skeleton of mouse oocytes [5, 11]. Note that not all activity is abolished in Fmn -/- and MyoV(-), presumably due to the remaining sources of non-thermal activity in the oocyte.

To develop a more intuitive picture of the activity we quantify the forces generated in the cell by calculating the cell force spectrum (S_{cell}) [16, 18, 19, 45]. S_{cell} directly represents the average total force on a vesicle from all stochastic sources (active and thermal) inside the cell. In analogy to the force on a simple spring, where the force is the stiffness multiplied by displacement ($F = \kappa \Delta x$, where κ is stiffness and Δx is displacement), we calculate $S_{\text{cell}} = (6\pi R)^2 |G^*|^2 \tilde{C}$ where $|G^*|^2$ represents the stiffness of the cytoplasmic-skeleton [18, 19, 49]. In our framework we separate the total force spectrum in the cell to be the sum of thermal forces and active forces ($S_{\text{cell}} = S_{\text{therm}} + S_{\text{active}}$) [45, 50]. The thermal force spectrum is calculated directly from the AMR measurements as $S_{\text{therm}} = 12\pi R G'' k_B T/\omega$ and represents the forces present at thermal equilibrium. The resulting force spectrum is shown in Fig 3C where at high frequencies the cell force spectrum (S_{cell}) is dominated by thermal forces (where $S_{\text{active}} \ll S_{\text{thermal}}$) as expected, but at lower frequencies ($f < 400$ Hz) active forces dominate ($S_{\text{active}} \gg S_{\text{thermal}}$) which result in higher total force experienced by vesicles in the cytoplasm over thermal equilibrium (lines represent theoretical model). To visualize the effect of thermal and active forces we show a representative trajectory of a vesicle (Fig. 3E, black). Based on our measured violation of FDT (Fig. 3A), we apply a filter to isolate the low-frequency (< 400 Hz) vesicle motion which is mainly due to active processes, and the high-frequency motion that is dominated by thermal fluctuations (Fig. 3E green, F respectively).

3.3 Modeling actively driven vesicle motion

Myosin-V is typically considered a directed transport motor. However, in prophase-I mouse oocytes, myosin-V drives vesicle motion in a non-directed fashion as evidenced by its sub-linear scaling of the mean-squared-displacement (Fig. 3D, blue). Previous work has also showed that myosin-V drives random motion of vesicles (active diffusion) on longer timecales of minutes [5]. To further illustrate this point, Fig. 4A(left) shows a schematic illustration of vesicles and actin filaments embedded in the oocyte interior. The complex mechanical environment is represented by a generic continuum (gray background). When myosin-V is attached to a vesicle and applies force on an actin filament, this force is transduced through the actin filament to a neighboring vesicle where it is bound by formin-2 (e.g. black arrows in Fig. 4A, right). This process occurs frequently throughout the oocyte interior resulting in randomly distributed force-dipoles (similar to myosin-II in some systems [17, 32]). Thus, each vesicle experiences forces in random directions due to the action of myosin-V throughout the network. This is represented by many actin filaments under force as shown in magenta in Fig. 4A(right). Therefore, due to the unique network connectivity in the cytoplasmic-skeleton, myosin-V motors drive active random motion in prophase-I mouse oocytes reminiscent of cytoplasmic stirring observed previously that was driven by myosin-II [32].

To gain access to the molecular-scale kinetics of the active processes driving the cytoplasmic interior of oocytes we developed a quantitative model describing vesicles embedded in a viscoelastic environment that are subjected to thermal and active forces. Here, the nonequilibrium processes, such as molecular motor activity, provide the active forces that reorganize the polymer cytoskeleton and drive motion of the vesicles. Our theoretical framework extends previous approaches for near-elastic networks [45, 49, 51] to include the complex mechanical properties measured experimentally (Fig. 2). The model describes a vesicle that is freely fluctuating in the viscoelastic continuum due to thermal forces, experiencing a local caging illustrated by the harmonic potential, with stiffness κ , in Fig. 4B(left) and governed by the dynamics described in

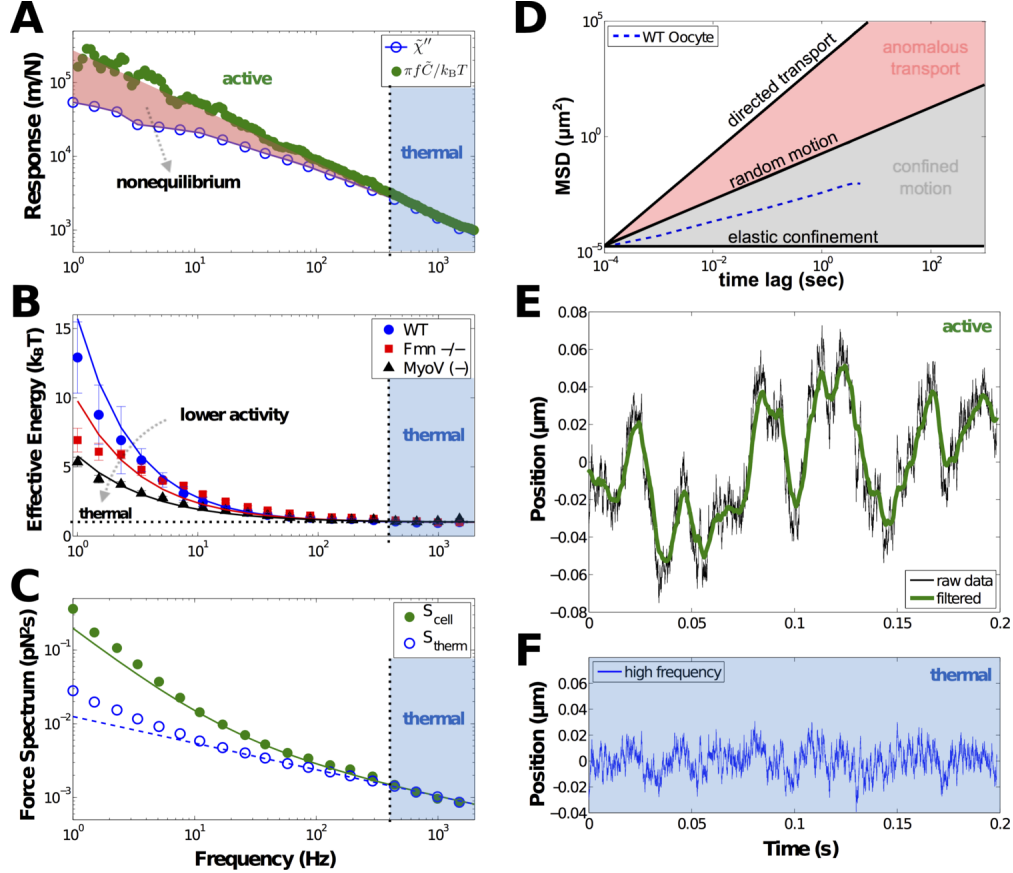


Figure 3: **Active force generation by myosin-V drives the cytoplasmic-skeleton out-of-equilibrium.** (A) At frequencies below 400 Hz the spontaneous motion of vesicles in oocytes (green circles) is larger than expected for thermal equilibrium (blue circles). This shows that active forces are contributing to vesicle motion in this regime as highlighted by the red shaded region. This is direct evidence of nonequilibrium behavior in the cytoplasmic-skeleton (via violation of the fluctuation-dissipation theorem (FDT)). At high frequencies the observed vesicle motion resembles thermal motion indicated by the blue shaded region. (B) WT oocytes (blue) are the furthest from equilibrium as shown by their higher effective energy. In the absence of actin (red) or when myosin-V is inactivated (black) the dynamic actin-myosin-V meshwork is compromised and oocytes have lower effective energy. Solid lines are theoretical fits (equations in SI, error bars = SEM). (C) The cell force spectrum (S_{cell}) experienced by vesicles is the sum of thermal forces (S_{therm}) and active forces (S_{active}) generated by molecular motors. At high frequencies S_{cell} (green) is dominated by S_{therm} (blue) and the two spectra coincide (blue shaded region). At lower frequencies S_{cell} is larger than S_{therm} showing the existence of additional active forces. Solid and dashed lines are theoretical predictions (equations in SI), low-frequency deviation is due to simple power-law model. (D) The mean-squared-displacement (MSD) of vesicles, calculated from trajectory data, indicates they undergo random-confined motion in the oocyte cytoplasmic-skeleton at short timescales. This behavior transitions to active diffusion at longer times [5], and is reminiscent of cytoplasmic stirring [32]. (E) When a representative trajectory (black) is filtered to remove the high-frequency thermal fluctuations the result is a smoothed trajectory (green) that represents actively driven motion. The difference between the true trajectory (gray) and the smoothed trajectory (green) recovers the high-frequency thermal fluctuations (blue) shown in (F).

equation 1. The molecular motor activity injects random forces into the network, which results in an active stochastic force on the cage, $\kappa\zeta_{\alpha}v_A$, that drives it to a new equilibrium position x_0 as in Fig. 4B(right) described by equation 2. These coupled equations of motion written in the Generalized Langevin approach

describe vesicle motion in the active viscoelastic environment of the cytoplasmic-skeleton,

$$\int dt' \gamma(t-t') \frac{dx}{dt} = -\kappa(x-x_0) + \xi \quad (1)$$

$$\int dt' \gamma(t-t') \frac{dx_0}{dt} = \kappa \zeta_\alpha v_A \quad (2)$$

where x is the position of the vesicle, ξ is Gaussian colored noise with correlations $\langle \xi(t)\xi(t') \rangle = k_B T \gamma(|t-t'|)$, as provided by the Fluctuation Dissipation Theorem [39], k_B is the Boltzmann constant, and T is the bath temperature of the environment. The viscoelastic material properties are described by, κ , the harmonic trap stiffness with center x_0 , and the memory kernel, $\gamma(t) = \gamma_\alpha t^{-\alpha} / \Gamma(1-\alpha)$, where Γ is the Gamma function, and $\zeta_\alpha = (\gamma_\alpha / \kappa)^{1/\alpha}$ is the microscopic timescale of the material. This memory kernel describes the measured mechanical properties of the cytoskeleton and influences the dynamics of both x and x_0 . The microscopic interpretation of κ is the local caging due to the cytoskeleton (as evident from the low frequency plateau in the measured shear modulus Fig. 2), and x_0 is the location of this cage. In the absence of active forces, the position of this local cage does not move ($\frac{dx_0}{dt} = 0$). When active forces do exist, as in living cells, they rearrange the cytoskeleton and drive motion of the cage ($\frac{dx_0}{dt} \neq 0$). The active force experienced by the cage results from the active burst velocity driven by molecular motors, v_A , which is a stochastic process consisting of alternating active and quiescent periods. During an active phase the active burst velocity, v_A , takes on a constant non-zero value, v , for a random exponentially distributed time of average value τ . During a quiescent phase the active burst velocity is 0 for an exponentially distributed random time τ_0 [45, 47, 49]. The active burst velocity is a zero-mean stochastic process with correlations $\langle v_A(t)v_A(0) \rangle = k_B T_A \exp(-|t|/\tau) / (\kappa \zeta_\alpha \tau)$, where $k_B T_A = \kappa \zeta_\alpha (v\tau)^2 / [3(\tau + \tau_0)]$ defines an active energy scale. Note that the dynamics of the joint process $\{x, x_0\}$ is not Markovian because of the memory kernel in the equations of motion.

From the generalized Stokes-Einstein relation, $\tilde{\gamma}(\omega) = 6\pi R \tilde{\eta}(\omega)$, where $\omega = 2\pi f$ is the frequency in radians/sec, R is the tracer's radius, the memory kernel can be associated with a complex modulus $G^* = G' + iG''$ of the form,

$$G'(\omega) = \frac{1}{6\pi R} \left[\gamma_\alpha \omega^\alpha \cos\left(\frac{\pi\alpha}{2}\right) + \kappa \right] \quad (3)$$

$$G''(\omega) = \frac{\gamma_\alpha}{6\pi R} \omega^\alpha \sin\left(\frac{\pi\alpha}{2}\right) \quad (4)$$

where G' is the real component of the complex modulus, and G'' is the imaginary component.

This model can directly separate the passive forces that originate from the thermal fluctuations of the medium and the active forces that depend on the energy consuming processes in the active material. Note that if the active force on the cage is zero, ($\kappa \zeta_\alpha v_A = 0$), then equation 2 is zero, and the equation of motion simplifies to confined viscoelastic Brownian motion (equation 1). If the active force is not zero, then it originates from molecular motor activity that has step-like velocity kinetics (Fig 4B, right inset). These force kicks drive the nonequilibrium fluctuations in our model.

The nonequilibrium properties of the motor activity are quantified by the deviation from the Fluctuation-Dissipation Theorem defined by a frequency dependent effective energy, E_{eff} , as discussed earlier. We compute it in terms of the microscopic ingredients of our theoretical model,

$$E_{\text{eff}}(\omega) = k_B T + \frac{1}{(\omega \zeta_\alpha)^{3\alpha-1} \sin(\pi\alpha/2)} \frac{k_B T_A}{1 + (\omega\tau)^2} \quad (5)$$

where $k_B T_A$ is the energy scale associated with the active process. The dynamics of the tracer can be written as: $x(t) = \int^t dt' \chi(t-t') F_{\text{cell}}(t')$, where $F_{\text{cell}} = \xi + \kappa x_0$ is the cell force which describes the thermal forces arising in the cell and the effect of the active forces via x_0 . This expression reveals one can access the cell force power spectrum S_{cell} by combining measurements of G^* and \tilde{C} . Explicitly, we calculate the cell force spectrum as $S_{\text{cell}} = \langle |\tilde{F}_{\text{cell}}|^2 \rangle = \langle |\tilde{\xi}|^2 \rangle + \kappa^2 \langle |\tilde{x}_0|^2 \rangle$ which corresponds to spectrum calculated previously $S_{\text{cell}} = \tilde{C} / |\tilde{\chi}|^2 = (6\pi R)^2 |G^*|^2 \tilde{C}$. Since we separate the thermal and active contributions to the force spectrum in our model, we are able to compute the explicit expressions for each,

$$S_{\text{therm}}(\omega) = 2\gamma_\alpha k_B T \omega^{\alpha-1} \sin\left(\frac{\pi\alpha}{2}\right) \quad (6)$$

$$S_{\text{active}} = \frac{2\kappa\zeta_\alpha}{(\omega\zeta_\alpha)^{2\alpha}} \frac{k_B T_A}{1 + (\omega\tau)^2} \quad (7)$$

The active force spectrum (equation 7) can now be used to extract force kinetics.

3.4 Extracting *in-vivo* molecular-scale force kinetics

By combining our model and experimental measurements, we can extract the force kinetics driving active mechanical processes in the oocyte. First, the mechanical measurements from AMR were fit equations 3 and 4 to determine the mechanical parameters: $\alpha, \zeta_\alpha, \kappa$ from the data shown in Figure 2A, B. Once the mechanics is determined, the remaining equations are largely constrained. The best fit of the data for effective energy (Figure 3B) is used to determine $k_B T_A$ in equation 5, where the fit is independent of τ when $\tau < 10$ ms. From fitting the active force spectrum we find that $\tau = 0.3$ ms to capture the high-frequency drop-off (Figure 4C). The fit parameters for the theoretical model are shown in Table 1. To summarize: $\alpha, \zeta_\alpha, \kappa$ are obtained from fitting AMR measurements of the mechanics (G', G''), T_A/T is obtained from fitting the effective energy data (E_{eff}), and τ is obtained from fitting the active force spectrum (S_{active}). Our model extracts the molecular-scale force kinetics directly from fitting the active force spectrum. As a result, we are able to capture the short timescale power-stroke (τ) of the active process, which is not possible from fitting the long timescale plateau of the *MSD* as done previously [18, 32]

To investigate how well our estimated kinetic parameters describe our experimental data we turn to Brownian dynamics simulations. We use the measured parameters (mechanics, kinetics, etc.) extracted from the AMR measurements and force spectrum to simulate vesicle dynamics via a stochastic equation of motion (see SM) using previously developed methods [52, 53]. These simulations of vesicle motion use exclusively values measured from experiment, without any free parameters. We analyze these simulations by calculating the full probability distribution of the simulated vesicle displacements (also known as van Hove Correlations) and compare them to our experimental measurements. We find that the statistics of the simulated vesicle motion is in excellent agreement with the measured spontaneous motion of vesicles in living oocytes (Fig 4D). Measured and simulated motion of vesicles is nearly identical including the central Gaussian region and the non-Gaussian tails (shaded red in Fig 4D) at short timescales. This non-Gaussian behavior is indicative of molecular motor activity and is dominated by the single most persistent molecular motor closest to the vesicle [54]. While our analytic model describes the mean values of the experimental measurements, these simulations exploit the full range of data by capturing the entire distribution of displacement correlations from experiments. Hence, the agreement found between simulations and experiment is non-trivial and serves as verification of our estimated kinetic parameters. These results show that our model of step-like active forces is able to capture the overall motion of vesicles (including higher-order statistics) embedded in the cytoplasmic-skeleton of living oocytes.

Table 1. Theoretical fit parameters

	mechanical properties			activity	
	α	ζ_α (s)	κ (pN $\cdot\mu\text{m}^{-1}$)	T_A/T	τ (ms)
WT	0.64	0.0657	20	5.5	0.30
Fmn2 -/-	0.6	0.103	18	5.0	0.15
MyoV (-)	0.57	0.163	27	3.8	0.1
	from AMR			from AMR/PMR	

4 Discussion

4.1 Myosin-V activity maintains a soft cytoplasmic-skeleton

Our mechanical measurements (AMR) indicate that when myosin-V activity is present the cytoplasmic-skeleton in oocytes is softer. The mechanism of how this occurs is not yet clear but may be related to the structural connectivity of the actin-myosin-V network. In our experiments, it is possible that when myosin-V is inactivated (MyoV(-)) it serves as a passive cross-linker that stiffens the environment. Since cross-linking leads to highly nonlinear stiffening [55], a small change in cross-linking could effectively increase the stiffness of the cytoplasmic-skeleton.

4.2 Intracellular activity dominates below 400 Hz in oocytes

In mouse oocytes, nonequilibrium activity emerges at higher frequencies ($f < 400$ Hz) than observed previously in other active systems ($f < 10$ Hz) [17, 18, 32]. This observation is not surprising since the timescale of FDT violation depends on both the mechanical properties and the typical timescale of the nonequilibrium activity of the system. The cytoplasmic-skeleton in oocytes is softer than previous systems [17, 43], and thus it is expected for the crossover to thermal motion to occur at higher frequencies (Fig. S4 in SM). Additionally, myosin-V kinetics are known to be faster than myosin-II [56], which was the driving force in previous experiments [17, 18, 32]. It is worth noting that while myosin-V is the dominant active force generator in the cytoplasm of prophase-I mouse oocytes [5], it is not the only force generator. Other sources of activity (e.g., polymerization, other molecular motors, etc.) also contribute to the amplitude of active forces measured.

4.3 Active force spectrum reveals molecular-scale kinetics of *in-vivo* myosin-V

To take a closer look at the extracted kinetics we consider the apparent active force experienced by the vesicle, $F = \kappa v \tau$, which we can substitute directly into the definition for the active temperature ($k_B T_A$) and rewrite the active force spectrum in a more intuitive way as,

$$S_{\text{active}} = \underbrace{\frac{1}{(\omega \zeta_\alpha)^{2\alpha}}}_{\text{mechanics}} \underbrace{\frac{1}{1 + (\omega \tau)^2} \frac{2(F \zeta_\alpha)^2}{3(\tau + \tau_0)}}_{\text{motor kinetics}} \quad (8)$$

The first factor in equation 8 depends on the mechanical properties of the cytoplasmic-skeleton while the second and third factor are related to the kinetic properties of the active processes. This illustrates that the active force spectrum is dependent on the force generation by molecular motors as well as the mechanics of the environment they must push against. The power-law scaling of the active force spectrum contains information about the underlying physics. At lower frequencies the active force spectrum scales as $f^{-2\alpha}$ reflecting the active forces pushing against the viscoelastic environment. At higher frequencies the active force spectrum is dominated by the kinetics of the active force generation process which scales as $f^{-(2\alpha+2)}$. This is illustrated in Fig. S3 where at low frequencies there is a power-law dependence of $-4/3$ consistent with the mechanics ($\alpha \approx 2/3$) and at high frequencies the power-law dependence is approximately $-10/3$ consistent with motor kinetics and mechanics. The crossover between these two regimes occurs at $1/\tau$ as shown approximately by the purple dotted line (Fig. S3).

Our predicted active force spectrum exhibits power-law scaling that is dependent on the mechanical properties of the system (α), in contrast to previous studies [16, 51, 57]. Previous theoretical developments predict an active force spectrum that scales as f^{-2} , which is independent of the mechanical properties [16], and a plateau (f^0) below a critical frequency (equation 2 in [32] and equation S1 in [18]). It is worth noting that in the near-elastic case ($\alpha \sim 0$), our model recovers the behavior observed in previous work [18, 32]. The divergence of the active force spectrum at low frequencies is consistent with our experimental measurements, and others, where a low-frequency plateau is not observed [18, 19, 21, 58].

The experimental measurements for the active force spectrum ($S_{\text{active}} = S_{\text{cell}} - S_{\text{therm}}$) and theoretical model are compared in Fig 4C. The low frequency power-law behavior is clearly seen, while at higher frequencies the active forces drop off rapidly which reflects the molecular motor statistics [59]. This allows us to calculate other kinetic parameters, such as the apparent active force amplitude, F , which is the average active force that an endogenous vesicle feels that drives its motion.

$$F = [3\kappa k_B T_A (\tau + \tau_0) / \zeta_\alpha]^{1/2} \quad (9)$$

where τ_0 is deduced from the single-molecule myosin-V duty cycle [60]. Once this force is known it is also straight-forward to calculate the expected average vesicle velocity,

$$v_v = \frac{F}{\kappa \zeta_\alpha} \quad (10)$$

which is a ratio of the driving force, and the resistance provided by the surrounding environment, $\kappa \zeta_\alpha$. Following this argument an approximate average step-size of the force kick can be computed by $\Delta x = F/\kappa$.

Thus, once the timescale of the force kick (τ) is extracted from equation 7, the apparent force felt by the vesicle (F), the expected vesicle velocity (v_v), and the step-size Δx can be deduced, which in our experiments closely agree with *in-vitro* values.

Our combined experimental and theoretical framework allows access to the molecular-scale kinetics via mesoscopic measurements of the active force spectrum (Fig. 4C). The active force spectrum, S_{active} , has only one free fitting parameter, τ , which corresponds to the molecular-scale activity. All other model parameters are fixed previously. In living oocytes we find that endogenous vesicles experience a force of $F \sim 0.4$ pN during a power-stroke of $\tau \sim 300$ μs duration, with a step-size of $\Delta x \sim 20$ nm. This is strikingly similar to single molecule myosin-V kinetics measured *in-vitro* [59–65]. In addition, we find that the predicted average vesicle velocity due to molecular motors is $v_v \sim 320$ nm/s which is in agreement with myosin-V velocity *in vitro* [61–63], as well as the velocity of myosin-V driven vesicles measured in *in-vivo* oocytes [5, 10]. Together, our results reveal that force kinetics of myosin-V motors are remarkably similar in *in-vitro* single-molecule studies and in *in-vivo* oocytes where they drive the composite cytoplasmic-skeleton out-of-equilibrium (Table 2).

Table 2. Molecular-scale force kinetics of myosin-V

	<i>in-vivo</i> oocytes	single-molecule myosin-V	reference
F (pN)	0.4	0-4	[59–62]
τ (μs)	300	160-1000	[60, 63, 64]
Δx (nm)	20	15-25	[60, 63–65]
v_v ($\mu\text{m/s}$)	320	270-480	[61–63]

5 Conclusion

We quantify the molecular-scale force kinetics of active diffusion driven primarily by myosin-V in mouse oocytes via experiments, theory, and simulation. We find that myosin-V kinetics is remarkably similar *in-vivo* as *in-vitro*, and that their activity can be extracted from cytoplasmic fluctuations. Our results demonstrate a widely applicable framework for connecting cellular scale phenomena to their underlying molecular force kinetics *in-vivo* and provide insight on the kinetic origin of active diffusion in mouse oocytes.

6 Author contributions

WWA and TB conceived and supervised the project. WWA, MB, MA, and MHV performed experiments. ÉF, NSG, PV, and FvW developed the theoretical model and performed simulations. WWA and ÉF integrated experiment and theory. All authors contributed to data analysis and/or interpretation. WWA and TB wrote the manuscript, which was seen and corrected by all authors.

7 Acknowledgements

We thank Jacques Prost, Cécile Sykes, Julie Plastino, and Jean-Francois Joanny for helpful discussions. We thank Melina Schuh (MRC Cambridge) for providing the MyoVb tail plasmid, Clément Campillo for help with synthetic vesicle experiments, and Amanda Remorino for critical reading of the manuscript. WWA is a recipient of post-doctoral fellowships from La Fondation Pierre-Gilles de Gennes and Marie Curie Actions. MA is a recipient of post-doctoral fellowships from the Ligue Nationale contre le Cancer and from the Labex MemoLife. MB is a recipient of an AXA Ph.D. fellowship. NSG gratefully acknowledges funding from the ISF (grant no. 580/12). MHV gratefully acknowledges the Ligue Nationale Contre le Cancer (EL/2012/LNCC/MHV). TB was supported by the French Agence Nationale de la Recherche (ANR) Grants ANR-11-JSV5-0002, and the Deutsche Forschungsgemeinschaft (DFG), Cells-in-Motion Cluster of Excellence (EXC 1003 – CiM), University of Münster, Germany.

References

- [1] Jonathon Howard. Mechanical Signaling in Networks of Motor and Cytoskeletal Proteins. *Annual Review of Biophysics*, 38(1):217–234, jun 2009.
- [2] L Blanchoin, R Boujemaa-Paterski, C Sykes, and J Plastino. Actin dynamics, architecture, and mechanics in cell motility. *Physiol Rev*, 94:235–63, 2014.
- [3] PA Janmey and CA McCulloch. Cell mechanics: integrating cell responses to mechanical stimuli. *Annu Rev Biomed Eng*, 9:1–34, 2007.
- [4] DA Fletcher and RD Mullins. Cell mechanics and the cytoskeleton. *Nature*, 463:485–92, Jan 2010.
- [5] M Almonacid, WW Ahmed, M Bussonnier, P Mailly, T Betz, R Voituriez, NS Gov, and MH Verlhac. Active diffusion positions the nucleus in mouse oocytes. *Nat Cell Biol*, 17:470–9, 2015.
- [6] CP Brangwynne, GH Koenderink, FC MacKintosh, and DA Weitz. Intracellular transport by active diffusion. *Trends Cell Biol*, 19:423–7, Sep 2009.
- [7] MC Munder, D Midtvedt, T Franzmann, E Nüske, O Otto, M Herbig, E Ulbricht, P Müller, A Taubenberger, S Maharana, L Malinowska, D Richter, J Guck, V Ziburdaev, and S Alberti. A pH-driven transition of the cytoplasm from a fluid- to a solid-like state promotes entry into dormancy. *Elife*, 5, Mar 2016.
- [8] BR Parry, IV Surovtsev, MT Cabeen, CS O’Hern, ER Dufresne, and C Jacobs-Wagner. The bacterial cytoplasm has glass-like properties and is fluidized by metabolic activity. *Cell*, 156:183–94, Jan 2014.
- [9] RP Joyner, JH Tang, J Helenius, E Dultz, C Brune, LJ Holt, S Huet, DJ Müller, and K Weis. A glucose-starvation response regulates the diffusion of macromolecules. *Elife*, 5, Mar 2016.
- [10] M Schuh. An actin-dependent mechanism for long-range vesicle transport. *Nat Cell Biol*, 13:1431–6, 2011.
- [11] Z Holubcová, G Howard, and M Schuh. Vesicles modulate an actin network for asymmetric spindle positioning. *Nat Cell Biol*, 15:937–47, 2013.
- [12] M Luksza, I Queguigner, MH Verlhac, and S Brunet. Rebuilding MTOCs upon centriole loss during mouse oogenesis. *Dev Biol*, 382:48–56, 2013.
- [13] V Nikolova, R Zhivkova, M Markova, T Topouzova-Hristova, A Mitkova, and S Delimitreva. Characterization of mouse oocytes and oocyte-cumulus complexes extracted for nuclear matrix and intermediate filaments (NM-IF). *Acta Morph. Anthropol*, 19:149–152, 2012.
- [14] A Chaigne, C Campillo, NS Gov, R Voituriez, J Azoury, C Umaña-Diaz, M Almonacid, I Queguiner, P Nassoy, C Sykes, MH Verlhac, and ME Terret. A soft cortex is essential for asymmetric spindle positioning in mouse oocytes. *Nat Cell Biol*, 15:958–66, 2013.
- [15] P Martin, AJ Hudspeth, and F Jülicher. Comparison of a hair bundle’s spontaneous oscillations with its response to mechanical stimulation reveals the underlying active process. *Proc Natl Acad Sci U S A*, 98:14380–5, 2001.
- [16] AW Lau, BD Hoffman, A Davies, JC Crocker, and TC Lubensky. Microrheology, stress fluctuations, and active behavior of living cells. *Phys Rev Lett*, 91:198101, 2003.
- [17] D Mizuno, C Tardin, CF Schmidt, and FC Mackintosh. Nonequilibrium mechanics of active cytoskeletal networks. *Science*, 315:370–3, Jan 2007.
- [18] M Guo, AJ Ehrlicher, MH Jensen, M Renz, JR Moore, RD Goldman, J Lippincott-Schwartz, FC Mackintosh, and DA Weitz. Probing the stochastic, motor-driven properties of the cytoplasm using force spectrum microscopy. *Cell*, 158:822–32, Aug 2014.

- [19] François Gallet, Delphine Arcizet, Pierre Bohec, and Alain Richert. Power spectrum of out-of-equilibrium forces in living cells: amplitude and frequency dependence. *Soft Matter*, 5(15):2947, 2009.
- [20] P Bursac, G Lenormand, B Fabry, M Oliver, DA Weitz, V Viasnoff, JP Butler, and JJ Fredberg. Cytoskeletal remodelling and slow dynamics in the living cell. *Nat Mater*, 4:557–61, 2005.
- [21] C Wilhelm. Out-of-equilibrium microrheology inside living cells. *Phys Rev Lett*, 101:028101, Jul 2008.
- [22] H. Turlier, D. A. Fedosov, B. Audoly, T. Auth, N. S. Gov, C. Sykes, J.-F. Joanny, G. Gompper, and T. Betz. Equilibrium physics breakdown reveals the active nature of red blood cell flickering. *Nat Phys*, 12(5):513–519, jan 2016.
- [23] MH Verlhac, JZ Kubiak, HJ Clarke, and B Maro. Microtubule and chromatin behavior follow MAP kinase activity but not MPF activity during meiosis in mouse oocytes. *Development*, 120:1017–25, 1994.
- [24] A Reis, HY Chang, M Levasseur, and KT Jones. APCcdh1 activity in mouse oocytes prevents entry into the first meiotic division. *Nat Cell Biol*, 8:539–40, 2006.
- [25] J Azoury, KW Lee, V Georget, P Rassinier, B Leader, and MH Verlhac. Spindle positioning in mouse oocytes relies on a dynamic meshwork of actin filaments. *Curr Biol*, 18:1514–9, Oct 2008.
- [26] M Schuh and J Ellenberg. A new model for asymmetric spindle positioning in mouse oocytes. *Curr Biol*, 18:1986–92, Dec 2008.
- [27] S Pfender, V Kuznetsov, S Pleiser, E Kerkhoff, and M Schuh. Spire-type actin nucleators cooperate with Formin-2 to drive asymmetric oocyte division. *Curr Biol*, 21:955–60, Jun 2011.
- [28] J Dumont, K Million, K Sunderland, P Rassinier, H Lim, B Leader, and MH Verlhac. Formin-2 is required for spindle migration and for the late steps of cytokinesis in mouse oocytes. *Dev Biol*, 301:254–65, Jan 2007.
- [29] M. L. Gardel, M. T. Valentine, J. C. Crocker, A. R. Bausch, and D. A. Weitz. Microrheology of Entangled F-Actin Solutions. *Phys. Rev. Lett.*, 91(15), oct 2003.
- [30] J Mas, AC Richardson, SN Reihani, LB Oddershede, and K Berg-Sørensen. Quantitative determination of optical trapping strength and viscoelastic moduli inside living cells. *Phys Biol*, 10:046006, 2013.
- [31] BH Blehm, TA Schroer, KM Trybus, YR Chemla, and PR Selvin. In vivo optical trapping indicates kinesin’s stall force is reduced by dynein during intracellular transport. *Proc Natl Acad Sci U S A*, 110:3381–6, Feb 2013.
- [32] N Fakhri, AD Wessel, C Willms, M Pasquali, DR Klopfenstein, FC MacKintosh, and CF Schmidt. High-resolution mapping of intracellular fluctuations using carbon nanotubes. *Science*, 344:1031–5, May 2014.
- [33] F Gittes and CF Schmidt. Interference model for back-focal-plane displacement detection in optical tweezers. *Opt Lett*, 23:7–9, 1998.
- [34] Timo Betz and Cécile Sykes. Time resolved membrane fluctuation spectroscopy. *Soft Matter*, 8(19):5317, 2012.
- [35] S Yamada, D Wirtz, and SC Kuo. Mechanics of living cells measured by laser tracking microrheology. *Biophys J*, 78:1736–47, Apr 2000.
- [36] Iva Marija Tolić-Nørrelykke, Emilia-Laura Munteanu, Genevieve Thon, Lene Oddershede, and Kirstine Berg-Sørensen. Anomalous Diffusion in Living Yeast Cells. *Phys. Rev. Lett.*, 93(7), aug 2004.
- [37] Y Jun, SK Tripathy, BR Narayanareddy, MK Mattson-Hoss, and SP Gross. Calibration of optical tweezers for in vivo force measurements: how do different approaches compare? *Biophys J*, 107:1474–84, Sep 2014.

- [38] MT Valentine, ZE Perlman, ML Gardel, JH Shin, P Matsudaira, TJ Mitchison, and DA Weitz. Colloid surface chemistry critically affects multiple particle tracking measurements of biomaterials. *Biophys J*, 86:4004–14, Jun 2004.
- [39] R Kubo. The fluctuation-dissipation theorem. *Rep. Prog. Phys.*, 29(1):255–284, jan 1966.
- [40] D. Mizuno, D. A. Head, F. C. MacKintosh, and C. F. Schmidt. Active and Passive Microrheology in Equilibrium and Nonequilibrium Systems. *Macromolecules*, 41(19):7194–7202, oct 2008.
- [41] FC MacKintosh, J Käs, and PA Janmey. Elasticity of semiflexible biopolymer networks. *Phys Rev Lett*, 75:4425–4428, Dec 1995.
- [42] David C. Morse. Viscoelasticity of Concentrated Isotropic Solutions of Semiflexible Polymers. 2. Linear Response. *Macromolecules*, 31(20):7044–7067, oct 1998.
- [43] M Guo, AJ Ehrlicher, S Mahammad, H Fabich, MH Jensen, JR Moore, JJ Fredberg, RD Goldman, and DA Weitz. The role of vimentin intermediate filaments in cortical and cytoplasmic mechanics. *Biophys J*, 105:1562–8, 2013.
- [44] WW Ahmed, É Fodor, and T Betz. Active cell mechanics: Measurement and theory. *Biochim Biophys Acta*, May 2015.
- [45] É. Fodor, M. Guo, N. S. Gov, P. Visco, D. A. Weitz, and F. van Wijland. Activity-driven fluctuations in living cells. *EPL*, 110(4):48005, may 2015.
- [46] T Betz, M Lenz, JF Joanny, and C Sykes. ATP-dependent mechanics of red blood cells. *Proc Natl Acad Sci U S A*, 106:15320–5, 2009.
- [47] E Ben-Isaac, Y Park, G Popescu, FL Brown, NS Gov, and Y Shokef. Effective temperature of red-blood-cell membrane fluctuations. *Phys Rev Lett*, 106:238103, Jun 2011.
- [48] J Prost, JF Joanny, and JM Parrondo. Generalized fluctuation-dissipation theorem for steady-state systems. *Phys Rev Lett*, 103:090601, Aug 2009.
- [49] É Fodor, K Kanazawa, H Hayakawa, P Visco, and Wijland F van. Energetics of active fluctuations in living cells. *Phys Rev E Stat Nonlin Soft Matter Phys*, 90:042724, 2014.
- [50] AW Lau and TC Lubensky. Fluctuating hydrodynamics and microrheology of a dilute suspension of swimming bacteria. *Phys Rev E Stat Nonlin Soft Matter Phys*, 80:011917, 2009.
- [51] FC MacKintosh and AJ Levine. Nonequilibrium mechanics and dynamics of motor-activated gels. *Phys Rev Lett*, 100:018104, Jan 2008.
- [52] Thierry Bochud and Damien Challet. Optimal approximations of power laws with exponentials: application to volatility models with long memory. *Quantitative Finance*, 7(6):585–589, dec 2007.
- [53] Andrew D. Baczewski and Stephen D. Bond. Numerical integration of the extended variable generalized Langevin equation with a positive Prony representable memory kernel. *The Journal of Chemical Physics*, 139(4):044107, 2013.
- [54] Toshihiro Toyota, David A. Head, Christoph F. Schmidt, and Daisuke Mizuno. Non-Gaussian athermal fluctuations in active gels. *Soft Matter*, 7(7):3234, 2011.
- [55] A. Sharma, A. J. Licup, K. A. Jansen, R. Rens, M. Sheinman, G. H. Koenderink, and F. C. MacKintosh. Strain-controlled criticality governs the nonlinear mechanics of fibre networks. *Nat Phys*, jan 2016.
- [56] MJ Tyska and DM Warshaw. The myosin power stroke. *Cell Motil Cytoskeleton*, 51:1–15, 2002.
- [57] Alex J. Levine and F. C. MacKintosh. The Mechanics and Fluctuation Spectrum of Active Gels †. *J. Phys. Chem. B*, 113(12):3820–3830, mar 2009.

- [58] Damien Robert, Thi-Hanh Nguyen, François Gallet, and Claire Wilhelm. In Vivo Determination of Fluctuating Forces during Endosome Trafficking Using a Combination of Active and Passive Microrheology. *PLoS ONE*, 5(4):e10046, apr 2010.
- [59] M Rief, RS Rock, AD Mehta, MS Mooseker, RE Cheney, and JA Spudich. Myosin-V stepping kinetics: a molecular model for processivity. *Proc Natl Acad Sci U S A*, 97:9482–6, Aug 2000.
- [60] G Cappello, P Pierobon, C Symonds, L Busoni, JC Gebhardt, M Rief, and J Prost. Myosin V stepping mechanism. *Proc Natl Acad Sci U S A*, 104:15328–33, Sep 2007.
- [61] AD Mehta, RS Rock, M Rief, JA Spudich, MS Mooseker, and RE Cheney. Myosin-V is a processive actin-based motor. *Nature*, 400:590–3, 1999.
- [62] C Veigel, S Schmitz, F Wang, and JR Sellers. Load-dependent kinetics of myosin-V can explain its high processivity. *Nat Cell Biol*, 7:861–9, 2005.
- [63] S Uemura, H Higuchi, AO Olivares, La Cruz EM De, and S Ishiwata. Mechanochemical coupling of two substeps in a single myosin V motor. *Nat Struct Mol Biol*, 11:877–83, 2004.
- [64] JR Sellers and C Veigel. Direct observation of the myosin-Va power stroke and its reversal. *Nat Struct Mol Biol*, 17:590–5, 2010.
- [65] C Veigel, F Wang, ML Bartoo, JR Sellers, and JE Molloy. The gated gait of the processive molecular motor, myosin V. *Nat Cell Biol*, 4:59–65, 2002.

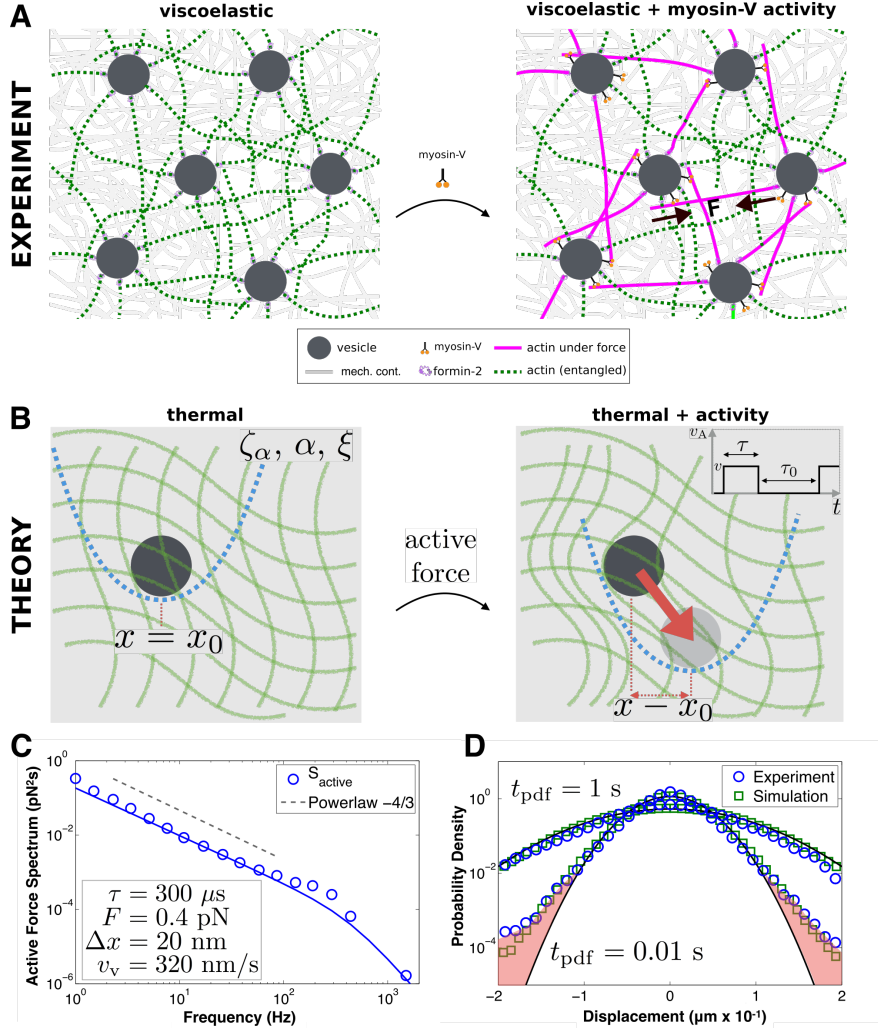


Figure 4: **A theoretical model of active mechanics connects *in vivo* measurements to molecular force kinetics.** (A) Vesicles (dark gray) are embedded in the complex mechanical continuum (gray background) of the oocyte interior. Actin filaments emanate from the the surface of vesicles creating an entangled network (green, left). Myosin-V motors generate force on actin (magenta, right) giving rise to forces throughout the network driving random motion of vesicles. (B) We model vesicles embedded in a mechanical continuum with local cage stiffness (κ) represented by the blue harmonic potential, viscoelastic dissipation (ζ_α, α), and thermal fluctuations (ξ) (left). Molecular motor activity rearranges the network through bursts of motion (v_A), resulting in displacement of the local cage (blue harmonic), which generates the active force ($\kappa\zeta_{\alpha}$, red arrow) that drives vesicle motion towards the local minimum (right)(inset indicates active force kinetics). (C) The active force spectrum (S_{active}) quantifies the forces on vesicles due to only active processes. Combined with our quantitative model we find that the vesicles are subject to 0.4 pN of force, during a power-stroke of length $\Delta x \sim 20$ nm and duration 300 μs , resulting in a vesicle velocity of 320 nm/s, which is strikingly similar to the kinetics measured for single molecule myosin-V *in-vitro* and the *in-vivo* vesicle velocity. The solid line is the theoretical fit (equation 7), and the dotted line is a $-4/3$ power-law consistent with the cytoplasmic-skeleton mechanics. (D) Simulated vesicle motion (green squares) agrees with experimental data (blue circles) for a wide range of timescales as shown by the probability distribution of displacements. This includes long timescale ($t_{\text{pdf}} = 1$ s) Gaussian behavior and short timescale ($t_{\text{pdf}} = 0.01$ s) non-Gaussian tails (indicated by red-shaded regions) that are indicative of molecular motor behavior, where t_{pdf} is the time-lag for calculation of the displacement correlations. Gaussian distributions shown in black. These results show that molecular level kinetics of active processes can be extracted from mesoscopic *in-vivo* measurements.